# Lessons from the analysis of a 3-D concrete shear wall

F.J. Vecchio†

*Department of Civil Engineering, University of Toronto, 35 St. George St. Toronto, Ontario, Canada M5S 1A4*

**Abstract.** A three-dimensional static nonlinear finite element analysis was performed on the NUPEC large-scale flanged shear wall, which was the subject of an international study program. Details of the constitutive models and analysis procedures used are provided, and the results of the analysis are presented and discussed. The analytical results are compared to the experimentally observed behaviour, and reasonable correlation is observed. Deficiencies in the modelling are identified. In addition, a parametric study is undertaken to investigate factors and mechanisms influencing both the observed behaviour and the calculated response. Finally, a cyclic load analysis of the wall is described and discussed. The paper serves to point out aspects in modelling that are critical to both producing realistic results, and correctly interpreting those results.

**Key words:** analysis; behaviour; cyclic; finite element; nonlinear; reinforced concrete; shear; structure; test; wall.

## 1. Introduction

In a study of the seismic design of shear walls in nuclear reactor buildings, the Nuclear Power Engineering Corporation of Japan (NUPEC) recently conducted an extensive experimental investigation. Two large-scale flanged shear walls (designated as ISP series) were subjected to dynamic loading conditions using a high performance shaking table (see Fig. 1). The results of the tests were made available to participants of the Seismic Shear Wall International Standard Problem (SSWISP) Workshop, so that the data might be used for verification of seismic response analysis codes.

At the request of the Brookhaven National Laboratory, a three-dimensional nonlinear static finite element analysis of the test specimen was undertaken. The shear wall was analyzed using the conceptual models, constitutive relations, and analysis software developed in-house at the University of Toronto. Previous application of these analysis tools to monotonically loaded shear walls were found to yield reasonably accurate results (Vecchio 1992).

This report summarizes the analytical formulations, finite element models, analysis results, interpretation of results, and relevant discussion pertaining to the ISP shear wall analyses. A parametric study of the factors influencing the behaviour of the test structure, using two-dimensional finite element analyses, is also presented.

† Professor

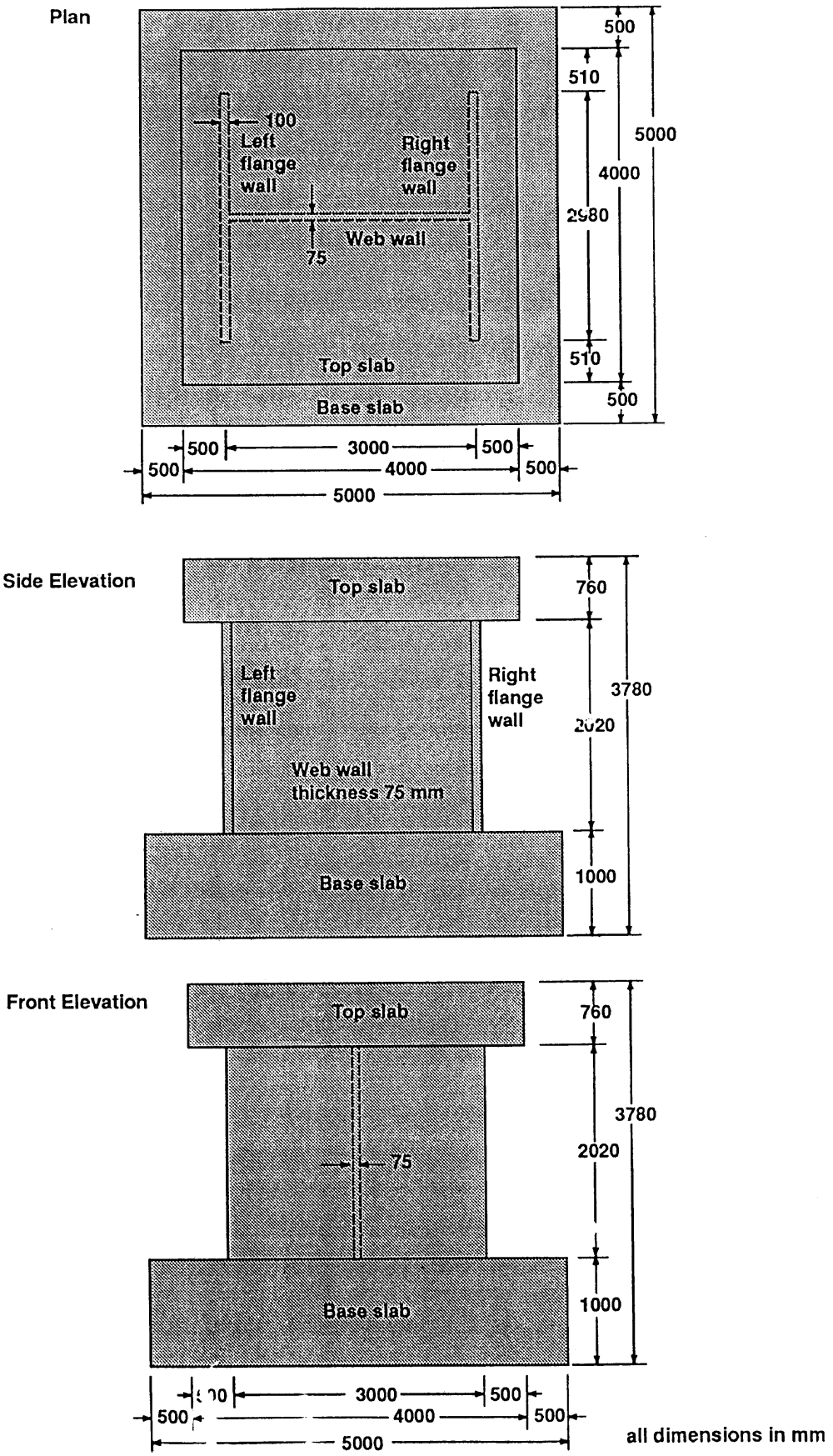


Fig. 1 Test specimen

## 2. Constitutive models

Concrete is modelled as an orthotropic nonlinear elastic material according to the Modified Compression Field Theory (Vecchio and Collins 1986). The constitutive equations for multiaxial stress states are based on modifications to a uniaxial stress-strain base curve (Hognestad parabola). Strength enhancement, arising from confining stresses are modelled by modifying the peak stress, and the strain at peak stress, of the parabolic base curve. The yield envelope proposed by Hseih *et al.* (1979) is used to determine the modifying peak stress factor. The modifying peak strain factor is determined from a fit to the data of Kupfer *et al.* (1969) for low peak stresses, and from a relationship according to Richart *et al.* (1928) for higher peak stress ratios. The negative gradient of the descending branch of the stress strain curve is based on the Modified Kent-Park model (Scott *et al.* 1982).

In tension-compression stress states, a compression reduction factor (or compression softening factor) is applied to the strength of the concrete after cracking. The compression reduction factor used is that proposed by Vecchio and Collins (1992). Note that according to the Vecchio/ Collins model, both the peak stress and peak strain of the base curve are modified. The reduction factor is a variable primarily dependent on the magnitudes of the strains transverse to the compression direction (i.e., by the degree of cracking).

The crack model used in the Modified Compression Field Theory (MCFT), assumes smeared rotating cracks. Cracking is assumed to occur normal to a principal stress direction, when that stress exceeds the uniaxial cracking strength of the concrete. While the constitutive relationships are formulated in terms of average stresses and average strains, local stresses at crack locations are also considered. The presence of average tensile stresses in the concrete implies local stress increases in the reinforcement at crack locations, and the presence of shear stresses on the concrete crack surfaces. Thus, the crack criteria includes a check that the local stresses in the reinforcement can be tolerated, and that the shear stresses on the crack surfaces are below a limiting value (Vecchio and Collins 1986). Otherwise, a shear slip can occur along the crack surfaces. The model is hypoelastic nonlinear; no attempt is made to reflect load/strain history in determining crack opening and closing. Cracks are assumed to 'heal' if the strains fall below the cracking strain.

The common approach of using a shear retention factor in modelling the shear stiffness of cracked concrete is not employed. Rather, in the manner of a true orthotropic elastic material, the shear stiffnesses are defined by the moduli of elasticity in the three principal directions, and by the associated Poisson's ratios. The Poisson's ratios are variable, modelled according to the data of Kupfer (1969), and are not necessarily set to zero after cracking.

Due to the influence of bond, post-cracking average tensile stresses can develop in the concrete between cracks. This so-called tension stiffening effect is modelled by adding a descending branch to the constitutive law for concrete in tension. The model proposed by Izumo *et al.* (1992) is used for the three-dimensional analysis presented herein.

Average stresses in the reinforcement are related to average strains using the standard elastic-plastic stress-strain relationship. A tri-linear curve is used to model strain hardening, although strain hardening was not relevant to the analyses herein. The MCFT currently does not model shear stiffness due to dowel action.

The MCFT, currently formulated for monotonically increasing quasi-static load conditions, assumes perfect bond to exist between the concrete and the reinforcement. Hence, no explicit bond-slip model is used, and no slip of embedded rebar is assumed to occur in a standard

analysis. However, tests indicate that the degradation in the bond between concrete and reinforcement, prevalent in dynamic and reversed cyclic loading conditions, has the effect of diminishing the development of post-cracking tensile stresses in the concrete. Thus, the effects of bond-slip can be approximated to some extent by discounting the tension stiffening effect; that is, by assuming no post-cracking tensile stresses in the concrete.

## 3. Finite element analysis procedure

Analyses were undertaken using program SPARCS, a three-dimensional nonlinear finite element program developed at the University of Toronto (Vecchio and Selby 1991) incorporating the constitutive relationships and conceptual models of the Modified Compression Field Theory. SPARCS employs a total load, secant stiffness approach in the formulation of its nonlinear analysis algorithm. An analysis usually begins by assuming linear elastic isotropic material properties. Element stiffness matrices are calculated and then the global stiffness is assembled. The load vector, which includes prestrain and expansion effects if any, is then formed. Nodal displacements are determined, from which one strain tensor is calculated for each element. Principal strains and corresponding directions are then found. Evaluation of the concrete and steel stresses using the constitutive models permits determination of secant moduli and, in turn, new material stiffness matrices. Average secant moduli are calculated; if they have converged to the specified limit, then the load stage is complete. Otherwise, the newly calculated material stiffness values are used to perform another linear elastic analysis. Normally, satisfactory convergence is achieved within 10 to 25 iterations. The control procedure in developing a load-deformation response history for a structure is by load control, with increments of load applied in each load stage.

SPARCS employs an 8-noded (24 degree of freedom) brick element which assumes linear displacement fields. As well, a 6-noded wedge element and a truss-bar element are available. Reinforcement is typically modelled as smeared within the elements, although it can be discretely represented using the truss-bar elements.

The equivalent two-dimensional nonlinear finite element program is TRIX (Vecchio 1989). It

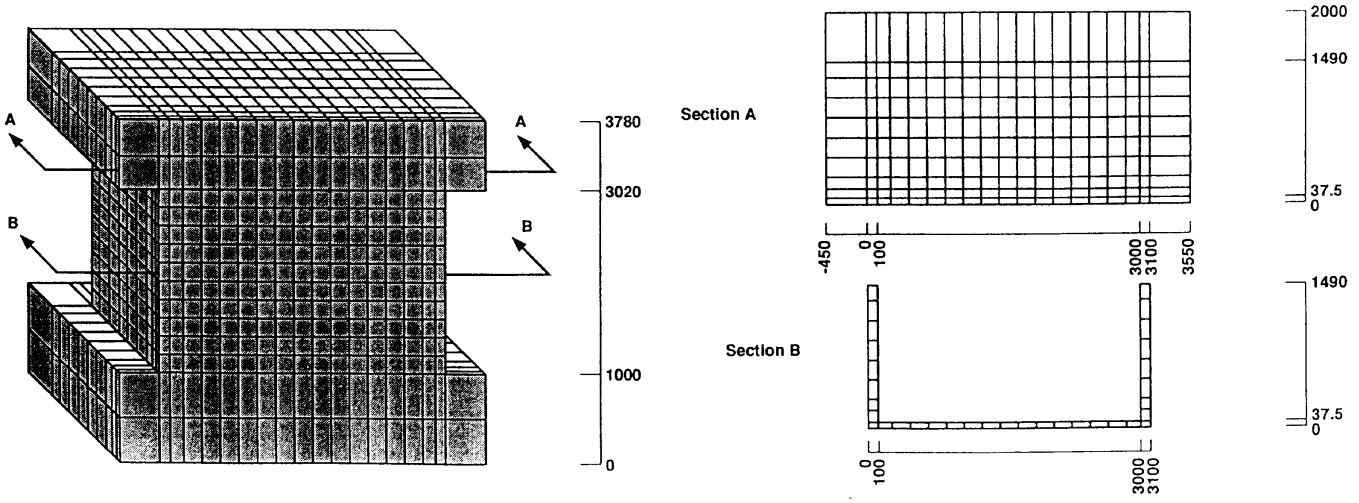


Fig. 2 3-D model of ISP shear wall

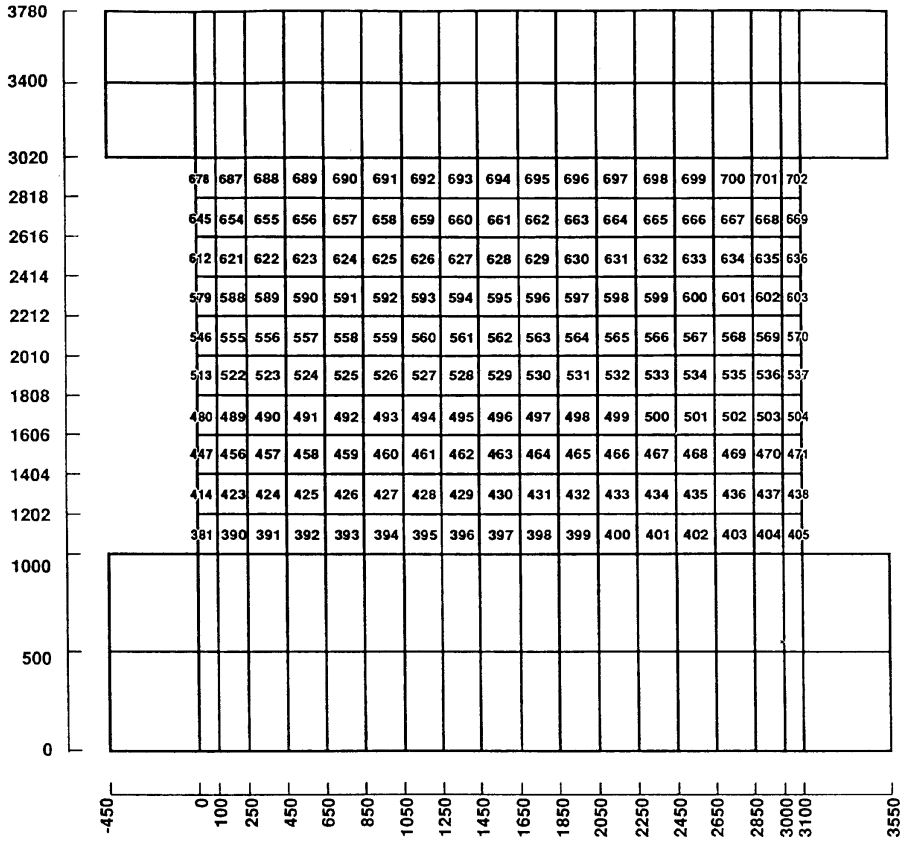


Fig. 3 Element numbering in web region

incorporates essentially the same material models and analytical formulations as SPARCS. TRIX was used for the 2-D parametric studies described later.

## 4. Modelling of test specimen

Taking advantage of symmetry, one-half of the structure was modelled using the element mesh shown in Fig. 2. A total of 1090 8-noded brick elements were used, requiring 1932 nodes and 5796 degrees of freedom. However, it should be noted that the large number of elements was a consequence of using an automatic mesh generating facility available, resulting in a disproportionate and unnecessary number of elements in the top slab and bottom slab regions. The top slab consumed 380 elements; the base slab required a similar amount; each flange consumed 90 elements, and the web was modelled with 150 elements. A significantly more efficient analysis, with no deterioration in accuracy, could be achieved through a coarser discretization of the top and bottom slabs. The element numbering scheme for the web portion of the structure is given in Fig. 3.

The structure was assumed fully restrained at all nodes along the bottom surface of the base slab. The total vertical load, having a constant value of 600 kN for the half-model, was uniformly distributed among the interior nodes at the mid-depth of the top slab. Similarly, the lateral loads were applied as uniformly distributed along the mid-depth of the top slab.

The concrete material properties used were as provided by NUPEC (1997). The concrete in the web/flange regions was modelled as having a compressive strength of 28.6 MPa, and a

tensile strength of 1.77 MPa. The strain at peak stress, taken from the cylinder curves provided, was 0.0025. The initial modulus of elasticity and the Poisson's ratio were 22,900 MPa and 0.155, respectively.

The reinforcement ratios in the web were 1.219% in both the horizontal and vertical directions. The reinforcement in the flange regions varied with position. At the intersection of the web and flange (a $75 \times 100$ mm area), the vertical reinforcement ratio was 1.707% (i.e., 4 rebars). For a distance of 250 mm out from the flange/web comer, the vertical reinforcement ratio was 0.760%. Beyond that point, to the outer tips, the vertical reinforcement ratio used was 0.366%. The horizontal reinforcement in the flanges was set at 1.371% to a distance 250 mm out from the web/flange comer, and at 0.914% in the areas beyond. The top and base slabs were nominally reinforced in all three directions. The reinforcement was modelled as elastic-plastic, with a yield stress of 384 MPa and a modulus of elasticity of 184,400 MPa.

Lateral load was applied in increments of 98.1 kN (10 tonf) per load stage, up to 981 kN. Beyond that point, the load step size was reduced to 49.0 kN (5 tonf). A tight convergence criteria was selected, requiring up to 30 iterations at each load stage. Using a MIPS Challenge M R4400/150 workstation, each load stage required up to 175 min CPU time, and approximately 8 hours real time to execute. Determination of maximum load was made from the flattening deformation response curves (e.g., displacements, strains in the reinforcement, shear strains in the concrete). At ultimate load, strains and displacements increased to extreme values (e.g., horizontal displacement of the top slab in excess of 200 mm), and was accompanied by an inability to converge to stable values.

## 5. Analysis results

The analysis of the ISP shear wall was done considering the full effects of tension stiffening, as would be appropriate under monotonically increasing load conditions. It should be emphasized that all the modelling decisions were made and all the analysis parameters were set before this initial (and only) analysis was executed. No 'fine-tuning' of the analysis was done subsequently in an attempt to obtain a better fit to the experimental results.

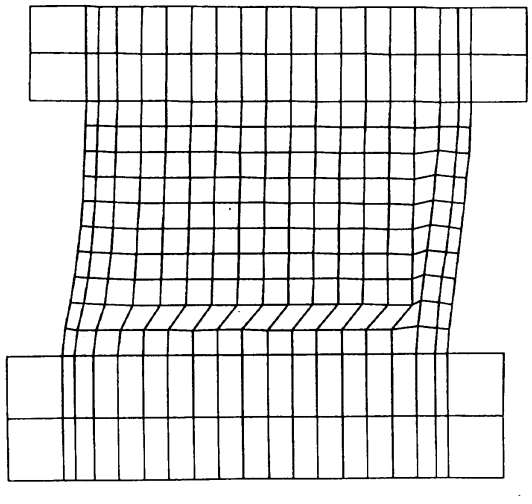

Fig. 4 Predicted failure shape from 3-D analysis

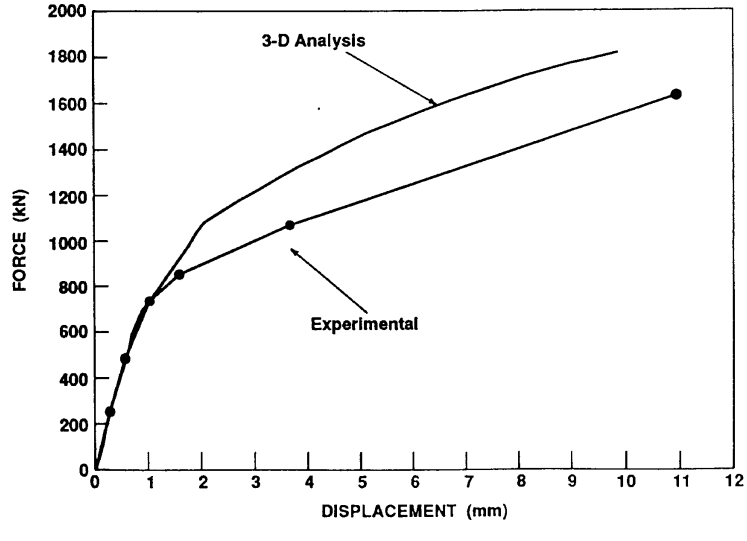


Fig. 5 Horizontal displacement of top slab

Under a monotonic lateral load applied at the mid-depth of the top slab, the shear wall was predicted to experience a brittle flexural/shear failure near the base. The predicted maximum strength of the wall was 1815 kN (185 tonf). The mode of failure, represented in Fig. 4, involved a shear/crushing failure of the concrete web leading to a shear failure plane forming approximately 300 mm above the base. Crushing of the concrete was also prevalent in the web regions adjoining the right flange. The web failure was partially initiated by the prior yielding of the reinforcement in the left flange. Yielding of the flange resulted in a deterioration of the clamping force, and thus a deterioration in the confinement effects, from which the web had benefitted.

The relatively brittle response of the wall is reflected in the load-deformation response curves. Shown in Fig. 5 is the horizontal displacement of the top slab (at its mid-depth). The first cracking sustained by the structure was predicted to be shear cracking in the web, in the lower left region centered around element 457 (see Fig. 3), at a load of 490 kN. By a load of 590 kN, the shear cracking had propagated essentially across the full width and full height of the web. At a load of 785 kN, the first flexural crack developed in the left flange, at the web-flange junction, just above the base (element 381). As loading increased, the flexural crack zone propagated outward and upward. At 1175 kN load, the horizontal flexural cracks had extended across the full width of the flange; the crack zone extended approximately one-third of the way up the flange. With increased loading, the crack zone continued to expand up the flange. It should be noted that the right flange, and the top and bottom slabs, remained essentially uncracked.

The flange wall vertical rebar was the first reinforcement to yield, occurring at a load of 1420 kN. Interestingly, however, the location of yielding was toward the outer tip of the flange, just above the base (elements 387-389). As load increased, the yielding zone gradually moved in toward the web. Yielding across the full width of the flange did not occur until a load of 1570 kN. The zone of yielding also propagated up the flange such that by ultimate load, yielding was widespread in the left flange. Fig. 6(a) shows the straining of the vertical reinforcement in the flange, at the web junction and just above the base (i.e., element 381). As ultimate load was approached, rapid and uncontrolled yielding of the reinforcement was predicted to occur. This ultimately contributed to the failure of the structure.

Yielding of the vertical reinforcement eventually migrated into the web zone. First yielding of the web wall vertical rebar occurred at a load of 1665 kN, in the bottom left comer area

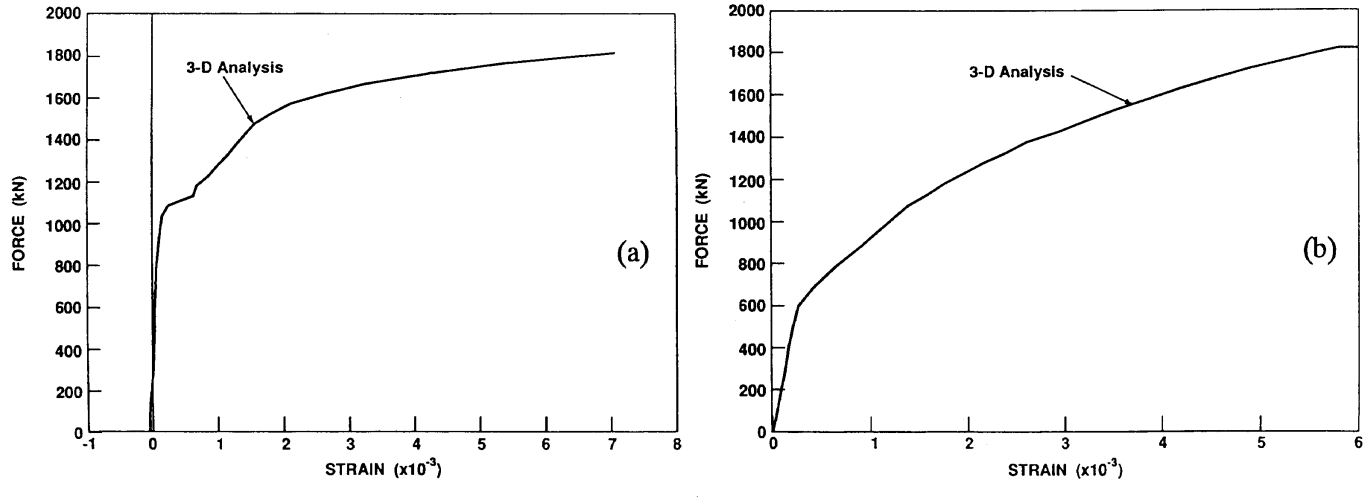


Fig. 6 (a) Vertical rebar strain-base of left flange, (b) shear strain in web

(elements 390, 391, 423). As load increased, the yield zone extended inward along the base. Failure of the wall ensued shortly after.

The web wall horizontal rebar was not highly stressed and did not yield. The greatest demand on the horizontal reinforcement was in the area adjacent to the right flange, about 700 mm above the base (elements 500 to 503). Here, the horizontal reinforcement acted together with the right flange to contain the outward thrust developed in the concrete compression strut that formed. Just prior to failure, the average stress in the horizontal reinforcement was about 67% of the yield stress. At crack locations, the maximum local stress in the horizontal reinforcement was approximately 75% of the yield stress.

The concrete in the web zone was highly stressed. The internal load-carrying mechanism that prevailed can be visualized as a simple strut-and-tie system, with the left flange representing a tension tie, the top and bottom slabs representing stiff chords, and a diagonal compression strut forming in the web from the top left comer to the bottom right corner. While the most highly stressed zone was that in the vicinity of the compression toe (elements 436, 469), the web was nearly uniformly stressed throughout, as it would be in the case of pure shear. It should also be noted that the zones immediately adjacent to the top and bottom slabs experienced less distress because of the out-of-plane confinement provided by the massive slabs. First crushing occurred in a zone about 400 mm above the base and 300 mm in from the right flange (elements 436, 437, 469), at a load of 1620 kN. The zone of crushing quickly expanded inward and upward. At 1720 kN, the concrete was extensively damaged in a large area spanning the lower right quadrant of the web. The concrete at about 300 to 500 mm up from the base (elements 434 to 437, 464 to 469) was in post-peak response, indicating the formation of a potential failure plane. The shear strain response of the concrete web, at element 437, is shown in Fig. 6(b). Excessive shear strains were apparent as the ultimate load was approached, indicating that a concrete shear failure was imminent.

The concrete in the compression flange was not highly stressed. At failure, the stress at the base of the flange was about 50% of the crushing strength, dropping rapidly to less than 10% of the crushing strength at distances 500 mm and greater above the base.

## 6. Discussion

It must be emphasized that the analysis presented simulates behaviour under the supposition of static monotonically increasing load. That the specimens were tested under dynamic cyclically-reversing loads raises some important factors that must be considered in trying to understand and correlate the predicted and observed behaviours.

Firstly, it is observed that the experimentally measured load-deformation responses are significantly less stiff than those predicted. The loss of tension stiffening effects under reversed cyclic load conditions has already been suggested as one possible reason for the discrepancy, accounting for a portion of the difference. However, a probably more significant factor is the degradation in the bond and anchorage of the reinforcement, particularly at the base. This behaviour is seen with cyclic loading conditions only, and would not have manifested itself had the wall been subjected to monotonic loads. The analyses conducted made no allowances for bond and anchorage slip at the base.

The analyses showed that the vertical reinforcement yielded across the full width of the left flange at approximately 1570 kN, and that yielding of the vertical reinforcement in the lower

left region of the web commenced shortly after at about 1620 kN. If the loads were then reversed, the vertical reinforcement in the right flange and right lower regions of the web could be expected to yield at similar load levels. However, the reinforcement on the left side, having undergone plastic yielding previously, would have retained some permanent offset strain. Through each cycle of loading, the offset strains resulting from yielding would tend to grow; this phenomenon is well-known and commonly referred to as the 'ratcheting effect'. The consequence is two-fold: i) a concentrated zone of damage is created near the base, in the yield regions, leading to a potential shear failure plane being established; ii) the increased strains result in a diminished confinement of the web, and an increased influence from compression softening, thus lowering the concrete web's ability to resist load. In situations where conditions lend themselves to this ratcheting effect, the reversed loading can result in a lowering of the ultimate load capacity and a change in the failure mode. It is interesting to note that the analyses predicted yielding of the vertical reinforcement in the flange and web at about the same load at which failure was observed in the test specimens. This would be consistent with observations from other experimental investigations; most notably with beam-column joints where this ratcheting behaviour leading to a shear-failure plane at the joint interface is well known. Thus, that the static analysis predicts a somewhat higher failure load (by approximately 12%), and a failure mode more in the nature of a shear-crushing of the web, is not unexpected. Further, one might speculate that a similar wall specimen tested under static loads would exhibit, to some degree, these variances relative to the dynamically tested specimens.

## 7. Parametric study

A parametric study was undertaken in an effort to more fully understand the behaviour of the test specimens, the factors influencing behaviour, and the factors influencing the analysis results. Due to the heavy demands on resources imposed by the three-dimensional models previously discussed, a two-dimensional model was used for the study. The finite element mesh used was of the same density as that used for the 3-D analysis; the same number and arrangement of elements was used in modelling the web portion of the wall. The flange portions, of course,

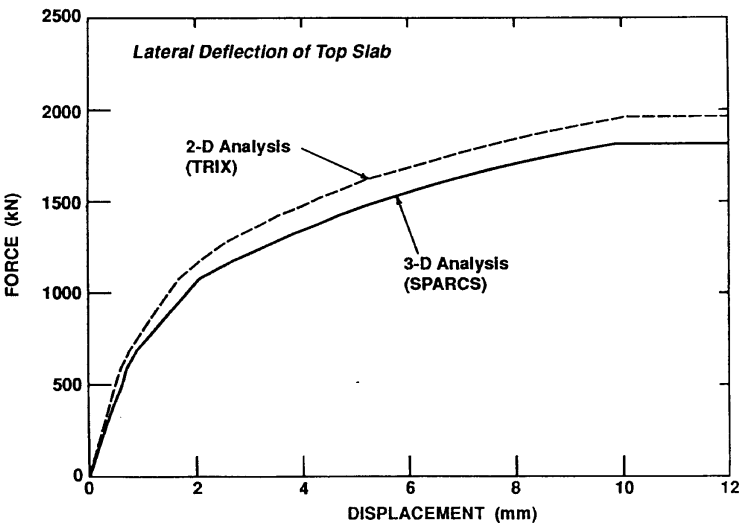


Fig. 7 Influence of three-dimensional effects

were not modelled out-of-plane and thus were represented by a single element of appropriate thickness. The material models and analysis parameters were as specified with the three-dimensional model. Analyses were performed using program TRIX. It is interesting to note that the TRIX analyses required approximately 1/50th the CPU time as a comparable three-dimensional analysis.

A two-dimensional analysis of the wall indicated a behaviour somewhat similar to that obtained from the three-dimensional analysis. The predicted lateral deflections of the top slab, from the two analyses, are compared in Fig. 7. It can be observed that: i) the 2-D analysis predicts an ultimate load capacity of 1960 kN, approximately 8% higher than that predicted by the 3-D analysis; and ii) the 2-D analysis predicts a substantially stiffer response. The failure mode in the 2-D analysis involves a sliding shear failure of the concrete web at an elevation of about 300 mm above the base.

Concentrating the full width of the flanges into a single element in the two-dimensional model has several significant implications. The thick, and thus very stiff, flange elements are assumed fully connected to the web elements. Thus, the degree of lateral and vertical confinement they provide to the web is over-estimated. Further, the shear lag effect that occurs in the out-of-plane direction in the three-dimensional model, and in reality, is not considered. Finally, the ability of the flange elements to carry a lateral shear is over-stated when full fixity to the web is assumed. These factors contribute to over-estimating both the strength and stiffness of the wall, relative to the three-dimensional analysis.

Not considering out-of-plane effects negates the triaxial confinement that occurs in the web regions adjoining the base slab. The ensuing strength enhancement in these regions is thus not fully taken into account. However, the effect quickly dissipates as one moves away from the base. As a result, the failure plane is unchanged relative to the results of the three-dimensional analyses.

In developing a two-dimensional model of the test structure, the question arises as to how much of the flange width is effective in contributing to the lateral load resistance of the wall. Four series of analyses were run, with the effective flange width (hence element thickness) modelled variously as 100% (2980 mm), 67% (2012 mm), 33% (1043 mm) and 0% (75 mm) effective. The corresponding lateral deflection responses at the top slab level are compared in Fig. 8(a). It can be seen that the assumption of a reduced effective flange width has a pronounced effect on the predicted response. Strength and stiffness are greatly diminished with each successive reduction in width. When the flange is considered totally ineffective, for example, wall strength is reduced by 55%. Also significant is the change in predicted failure mode. With a decreasing flange width, the failure mode becomes more flexural in nature. Increasing tensile strains and pronounced yielding are observed in the left flange at earlier loads, and eventually capacity is governed by a concrete crushing failure in the right flange.

The assumption of post-cracking tensile stresses in the concrete has a measurable impact on the computed stiffness of the structure and, to a lesser extent, on the computed strength. To get a firmer understanding of the significance of this mechanism, and to test the sensitivity of the analysis results to the type of model used, four analysis series were undertaken. The following tension stiffening models were used: i) the Izumo *et al.* model, shown to provide reasonable results in flexure-dominated conditions; ii) Vecchio-Collins model, which seems to provide the most accurate simulations in membrane stress conditions but tends to overestimate stiffness under flexural conditions; iii) the Collins-Mitchell model, which serves as a good general purpose model and provides reduction factors for long term and cyclic loading conditions; and

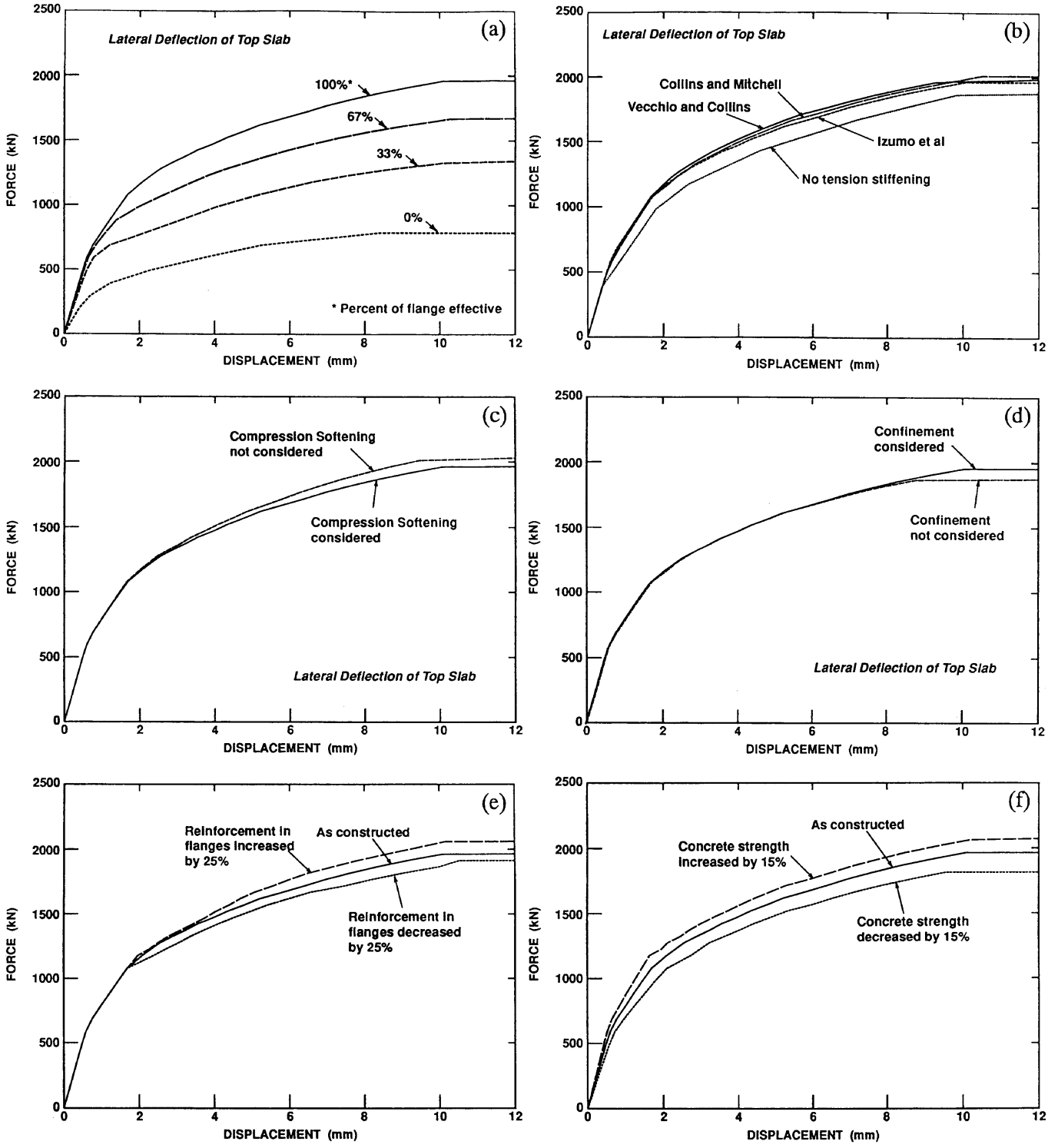


Fig. 8 (a) Influence of effective flange width, (b) Influence of tension stiffening, (c) Influence of compressive softening, (d) Influence of confinement, (e) Influence of vertical reinforcement in flange, (f) Influence of concrete strength

iv) no tension stiffening effects after cracking. The resulting lateral load-deflection responses are compared in Fig. 8(b). As can be seen, the responses predicted using the three alternative tension stiffening models exhibit only minor differences. The Vecchio-Collins model is stiffest, and the Izumo *et al.* model is least stiff, as would be expected. However, the differences in

deflections never exceed 10% at any load level. Conversely, ignoring tension stiffening effects results in deflections increased by as much as 30% at intermediate and higher load levels. The predicted strength of the wall is also affected somewhat, since the degree of deflection sustained impacts on the degree of containment afforded the web. However, the influences are minor, except when tension stiffening is discounted altogether. In the latter case, the predicted strength is reduced by about 5%. There is no influence on the predicted failure mode.

As is well documented in the literature, the effective compressive strength of concrete is reduced in the presence of transverse tensile strains. For elements subjected to membrane shear, compression softening can significantly affect the strength, stiffness and failure mode of the structure. To investigate the magnitude of the effect in this case, two analyses were done: one using the Vecchio-Collins 1992 model for compression softening; and one in which no compression softening effects were considered. The predicted load-deformation responses are compared in Fig. 8(c). When compression softening is considered, only a slight degradation in stiffness is observed at later load stages. Further, the ultimate load capacity is reduced by a mere 3%. Thus, for this structure, the compression softening effect is not significant. The influence is minimal because neither the vertical nor horizontal reinforcement in the highly stressed regions of the web yielded. The transverse tensile strains remained relatively small, and hence the reductions in compressive strength and stiffness were small. The compression softening effect becomes much more pronounced in situations where the tensile strains become large, as when there is yielding of either the horizontal or vertical reinforcement in the membrane elements.

The analysis results discussed previously indicated that concrete strength enhancement due to confinement affected the strength and failure mode of the wall to some degree. Recalling the results of the both the 2-D and 3-D models, confinement effects introduced by the massive base stiffened the adjoining web regions and pushed the failure plane up the wall away from the base. Furthermore, the vertical and lateral confinement provided by the stiff flange regions allowed the concrete in the web to achieve a higher strength before failing. To further test the role of confinement effects in the response of the wall, an analysis was done in which the concrete confinement effects were removed. That is, no strength or stiffness enhancement was allowed due to biaxial or triaxial compression effects. The resulting load deformation response of the wall is compared in Fig. 8(d) to the standard case (which allows for confinement effects). It is seen that neglecting confinement effects results in a modest decrease in the load capacity of the wall, with a reduction of about 5%. The failure mode is essentially unchanged. Also, there is virtually no effect on the stiffness of the load-deformation response prior to failure.

The three-dimensional analyses suggested that the failure of the wall was governed by the shear-crushing failure of the concrete in the web, occurring after yielding of the vertical reinforcement in the left flange. Once the flange lost its ability to clamp down on the web, the reduced confinement of the web instigated failure. Would averting yield in the flanges, by increasing the amount of reinforcement provided, significantly increase the strength and stiffness of the wall? To address this question, the standard 2-D analysis was coupled with two additional analyses: one with 25% more reinforcement provided in the flanges; and one was 25% less reinforcement. The results are shown in Fig. 8(e). It is seen that the strength and stiffness are not affected in a degree proportional to the amount of reinforcement provided. The increase of 25% in reinforcement area results in an increase in load capacity of about 5% relative to the standard case. Similarly, a decrease in reinforcement of 25% results in a decrease in capacity of about 3%. In all cases, the reinforcement in the flanges continues to yield and the failure mode remains

unchanged. Deflections are influenced to only minor degrees as well. Thus, while yielding of the reinforcement in the flanges contributes ultimately to a shear failure of the web, it is not a major influencing factor.

From earlier analyses it has been concluded that failure of the wall was dictated by a shear failure of the concrete web, and that compression softening effects and loss of confinement due to yielding of the tension flange played only minor roles. This then suggests that the concrete failure in the web was a result of the direct compressive strength being exceeded. If so, changes in the strength of the concrete should have a noticeable effect on the strength of the wall. To test this hypothesis, another set of analyses was undertaken. In addition to the standard case, two other analyses were performed: one with the compressive strength of the concrete in the wall increased by 15%; and another with the strength decreased by 15%. The resulting lateral load-deformation responses are given in Fig. 8(f). It is seen that the wall strength is influenced by the concrete strength to a much larger degree than it was by the flange reinforcement amount. A 15% increase in concrete strength brings an 8% increase in the wall's load capacity; a 15% decrease in concrete strength results in a 8% decrease in wall capacity. Deflections are similarly affected. Given that the wall capacity is influenced by other structural parameters as well, including the amounts of vertical and horizontal reinforcement in the web and the area of the compression flange, the correlation between concrete strength and wall load capacity is strong. The indication is that the concrete strength is being fully utilized.

## 8. Influence of mesh size

With respect to the discretization of the web wall, the finite element mesh used for the two-dimensional analyses was purposely made similar to that used for the three-dimensional analyses. Considering the stiff nature of the top and bottom slabs, and the low height-to-width ratio of the wall, one can expect boundary effects to be significant. Given that the finite elements used were low-powered, one must consider whether the mesh used was sufficiently fine. To this end, two additional 2-D analyses were undertaken with progressively finer meshes. Recall that the original 2-D mesh contained 246 elements. The additional analyses employed meshes of 540 elements and 984 elements, respectively; roughly, 2 times and 4 times the density of the original

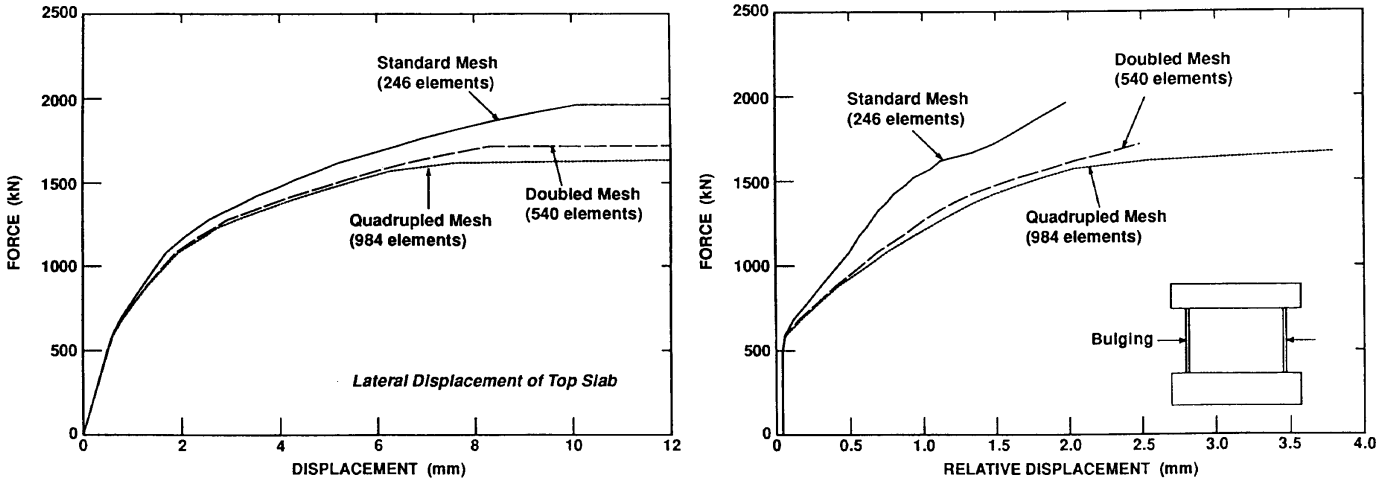


Fig. 9 (a) Influence of mesh size, (b) predicted bulging of web at mid-height

mesh.

Compared in Fig. 9(a) are the predicted load-deflection responses of the top slab. It is immediately evident that there are significant differences in the computed responses. The finer meshes result in: i) lower cracking stresses; ii) reduced stiffness after cracking; and iii) a lower ultimate load capacity. Post-cracking deflections are increased by as much as 50% in the later load stages, and the ultimate load is reduced by 17%. Note that the 'doubled mesh' and 'quadrupled mesh' give essentially similar results, suggesting that a further refinement of the mesh is not necessary.

The finer meshes are better able to capture the lateral expansion of the web wall that occurs away from the constrained top and bottom ends. Shown in Fig. 9(b) is the predicted bulging of the wall at mid-height; that is, the relative horizontal displacement between the two flanges in the plane of the web. The finer meshes predict considerably higher expansions (i.e., tensile strains). The result is an increased compression softening effect in the web concrete, higher stresses in the web reinforcement, and higher stresses in the restraining flanges. These effects result in a decreased stiffness, and an earlier failure of the concrete. The predicted modes of failure are not significantly different, however.

## 9. Cyclic load analysis

The above analysis results were submitted to the ISP prediction competition in September 1995. Since then, work has progressed towards implementing cyclic load capabilities into the finite element programs. Appropriate constitutive models, loading/unloading rules, and analysis algorithms have been developed and incorporated into the 2-D program TRIX (Vecchio 1997). Work is nearing completion towards a similar revision of the 3-D program SPARCS.

A 2-D cyclic load analysis was subsequently undertaken for the ISP shear wall. The double density mesh was used, owing to the findings of the mesh density study reported above. All other material properties and analysis parameters were as before. The analysis was done in displacement imposed mode, with displacement amplitudes increasing by 1.0 mm per cycle. One

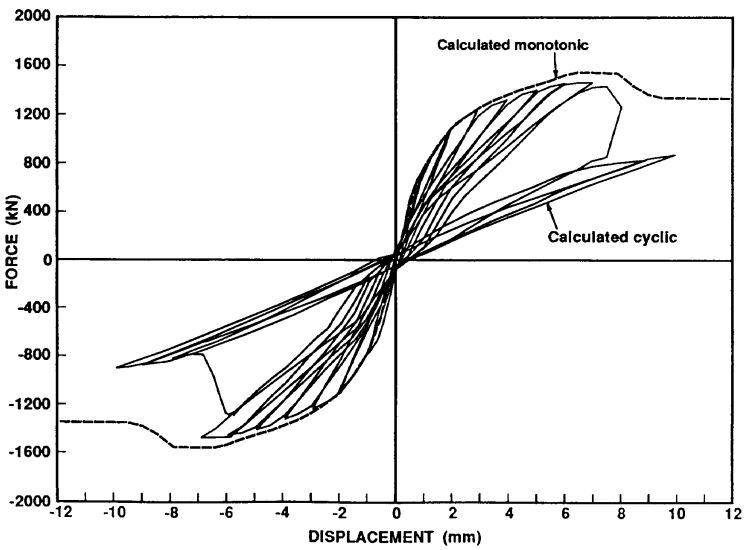


Fig. 10 2-D cyclic load analysis of ISP wall

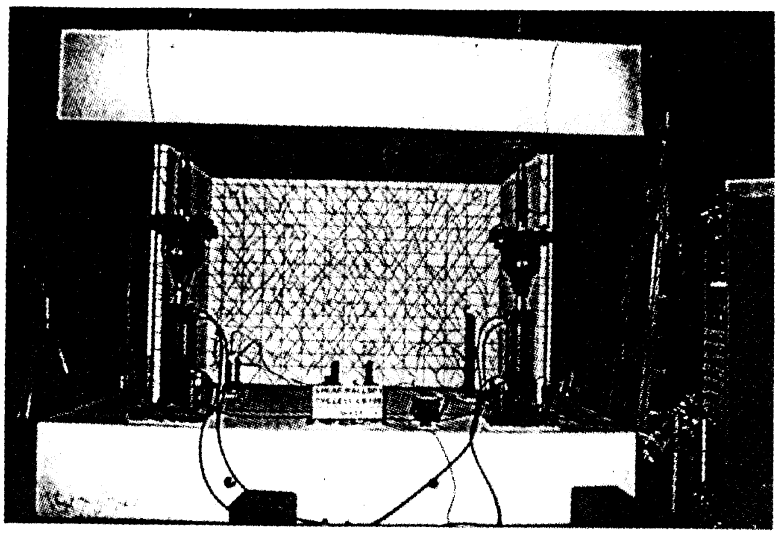

Fig. 11 University of Toronto shear wall DP1

cycle per amplitude level, and a size of 0.25 mm, were used.

A measurable reduction in both the strength and stiffness of the wall was seen to result from the imposition of cyclic loads. What is particularly relevant, in the context of previous discussions, is that first yielding of the vertical reinforcement in the flanges occured during the first +/− 6.0 mm excursion. At this level, the lateral load on the structure was 1460 kN. During the subsequent 7.0 mm excursion, strains in the reinforcement accumulated with no increase in corresponding peak lateral load. A shearing failure of the concrete occured along the base and along the flange wall joint, as before, during the 8.0 mm cycle. Thus, the 'ratcheting' mechanism previously discussed became a factor in the analysis results. It should also be noted that the cyclic load analysis results were a slightly better correlation to the experimental results. However, the inaccuracies relating to the improper representation of three-dimensional effects remained a significant factor.

To further investigate cyclic load mechanisms and post-peak ductility mechanisms, an experimental program is underway. Two test specimens similar to the ISP are being constructed and tested. To complement the NUPEC data, one of these will be tested under reversed cyclic quasi-static loads, and one will be subjected to monotonically increasing imposed displacements. The results will assist in better quantifying relevant behaviour models.

## 10. Conclusions

From the three-dimensional nonlinear static finite element analyses undertaken of the ISP shear wall, the following conclusions may be drawn:

i) The wall strength is predicted to be 1815 kN under monotonically increasing lateral load; this is approximately 12% greater than the experimentally observed value with the wall tested under dynamic cyclically reversing loads.

ii) The predicted load-deformation responses agree well with the observed behaviour before cracking; however, the cracking load and post-cracking stiffness are overestimated. The degradation of tension stiffening effects partially accounts for the decreased stiffnesses observed in the test specimens. Deterioration in the bond and anchorage of the reinforcement, which was

not considered in the analyses, is likely a contributing factor as well.

iii) The predicted failure mode is one involving a shear-crushing of the concrete web, resulting in a shear plane approximately 300 mm above the base, occurring after yielding of the reinforcement in the tension flange. The predicted mode of failure is in reasonable agreement with the observed failure.

iv) Three-dimensional effects are significant. The flanges are near fully effective in contributing load resistance to the structure. The massive top and bottom slabs provide out-of-plane confinement to the web wall, enhancing the strength of the adjoining concrete web elements.

v) The sequence and location of yielding in the flange and web regions were such that likely 'ratcheting effects' influenced the failure mode and load capacity of the wall. This phenomenon is commonly observed in beam-column joints subjected to cyclic loads. Its effect is to produce a well-defined shear failure plane across the zone of yielding, at loads slightly higher than those required to yield the reinforcement, sequentially, on both faces of the element.

From the parametric study undertaken, using two-dimensional nonlinear static finite element analyses, the following conclusions are supported:

i) Two-dimensional analyses fail to capture some important three-dimensional effects, such as the out-of-plane confinement provided by the base slab and shear lag effects in the flange walls. They also lead to an over-estimation of the lateral and horizontal confinement of the web provided by the flanges, and an over-estimation of the contribution of the flange elements to the lateral shear stress distribution. The result is a slightly stronger and stiffer response than obtained using a three-dimensional analysis. However, the loss in accuracy is not severe, and the failure mode remains predicted well.

ii) In modelling the thickness of the flange elements, an effective thickness of between 67% and 100% of the width of the flanges appears to be appropriate. The flanges are nearly fully effective.

iii) The choice of a tension stiffening model, among several available, does not significantly affect behaviour. However, ignoring tension stiffening effects results in substantial increases in post-cracking deflections, and a slight lowering of the ultimate load capacity.

iv) Compression softening effects (i.e., the degradation in compressive strength of cracked concrete due to the influence of transverse tensile strains) is not a significant influencing factor for this test specimen.

v) Confinement effects have a minor influence, resulting in a slightly increased load capacity and a positioning of the failure plane up away from the base.

vi) The amount of vertical reinforcement provided in the flanges is not a significant influencing factor, although yielding of this reinforcement immediately precedes the web shear failure.

vii) The compressive strength of the concrete in the web is fully utilized at ultimate load. Increasing or decreasing the concrete strength significantly affects the predicted failure load of the structure. Thus, the strength of the wall is most governed by the strength and thickness of the web. The vertical and horizontal reinforcement in the web are of sufficient amounts to not yield. The flanges are of sufficient width, and sufficiently reinforced, to not precipitate a flexural failure.

viii) The element mesh used to model the web wall, in both the standard two- and threedimensional analyses, was too coarse. Analytically, there was insufficient freedom for the mid-height regions of the web to overcome the restraint imposed by the stiff top and bottom slabs. A finer mesh predicts a considerably less stiff response, and a significantly lower load

capacity.

## Acknowledgements

The Nuclear Power Engineering Corporation (NUPEC) of Japan tested the shear walls, and provided the data for use as an International Standard Program (ISP) study. Brookhaven National Laboratory (BNL) of Upton, N.Y., USA sponsored the analyses discussed herein. The support received from both organizations is gratefully acknowledged.

## References

Collins, M.P. and Mitchell, D. (1991), *Prestressed Concrete Structures*, Prentice-Hall, New Jersey.

Hsieh, S.S., Ting, E.C. and Chen, W.F. (1979), "An elastic-fracture model for conrete", *Proc. 3rd Eng. Mech. Div. Spec. Conf., ASCE*, Austin, Texas, 437-440.

Izumo, J., Shin, H., Maekawa, K. and Okamura, H. (1992), "An analytical model for RC panels subjected to in-plane loads", *Concrete Shear in Earthquake*, Elsevier Applied Science, London, 206-215.

Kupfer, H., Hilsdorf, K.H. and Rusch, H. (1969), "Behaviour of concrete under biaxial stress", *J. Amer. Concrete Inst.*, **66**(8), 656-666.

Nuclear Power Engineering Corporation (1996), "Comparison report, seismic shear wall ISP, NUPEC's seismic ultimate dynamic response test", Report No. NU-SSWISP-DO14.

Richart, F.E., Brandzaeg, A. and Brown, R.L. (1928), "A study of the failure of concrete under combined compressive stresses", Bulletin No. 185, Univ. of Illinois Engineering Experimental Station, Urbana, Illinois.

Scott, B.D., Park, R. and Priestley, M.J.N. (1982), "Stress-strain behaviour of concrete confined by overlapping hoops at low and high strain rates". *J. Amer. Concrete Inst.*, **79**(1), 13-27.

Vecchio, F.J. and Collins, M.P. (1986), "The modified compression field theory for reinforced concrete elements subjected to shear", *J. Amer. Concrete Inst.*, **83**(2), 219-231.

Vecchio, F.J. (1989), "Nonlinear finite element analysis of reinforced concrete membranes", *Amer. Conc. Inst. Structural J.*, **86**(1), 26-35.

Vecchio, F.J. and Selby, R.G. (1991), "Towards compression field analysis of reinforced concrete solids", *J. Struct. Engrg., ASCE,* **117**(6), 1740-1758.

Vecchio, F.J. (1992), "Finite element modelling of concrete expansion and confinement", *J. Struct. Engrg., ASCE,* **118**(9), 2390-2406.